

# Electronic transport of Au-adsorbed Si(111)- $\sqrt{3}\times\sqrt{3}$ -Ag: Metallic conduction and localization

Canhua Liu,<sup>\*</sup> Iwao Matsuda,<sup>†</sup> Shinya Yoshimoto,<sup>†</sup> Taizo Kanagawa, and Shuji Hasegawa  
*Department of Physics, School of Science, University of Tokyo, 7-3-1 Hongo, Bunkyo-ku, Tokyo 113-0033, Japan*  
 (Received 2 April 2008; published 23 July 2008)

The electrical conductance of Au-adsorbed Si(111)- $\sqrt{3}\times\sqrt{3}$ -Ag surface was studied as a function of temperature (110–300 K) by a method of micro-four-point probe. In the pristine surface without Au adsorbates, the surface electrical conductance was inversely proportional to the temperature, indicating a metallic nature dominated by electron-phonon scattering. After deposition of small amounts of Au adsorbates [0.02 and 0.14 monolayer (ML)], the surface electrical conductance decreased with temperature, exhibiting a nonmetallic behavior in spite of nearly free-electron and metallic surface bands still existing. It is explained by localization of surface-state electrons due to randomly dispersed Au nanoclusters at 0.02 ML coverage and due to disordered and high-density domain boundaries in the  $\sqrt{21}\times\sqrt{21}$  superstructure at 0.14 ML coverage of Au.

DOI: 10.1103/PhysRevB.78.035326

PACS number(s): 73.20.-r, 73.25.+i, 72.15.Rn, 73.63.-b

## I. INTRODUCTION

The electronic transport properties of surfaces and ultrathin films have received much attention because of their strong correlation with unique properties of materials in reduced dimension. The electronic transport properties are mainly determined by electronic band structures, especially by the density of states (DOS) at Fermi level ( $E_F$ ).<sup>1</sup> Since the detailed surface structure and morphology can modify the DOS at surface dramatically, direct measurements of the surface electrical conductance is a challenging way of studying fundamental transport physics.<sup>2,3</sup> Recently, for example, Tanikawa *et al.*<sup>4</sup> succeeded in detecting directly the electrical conductivity through the surface states of the Si(111)-4 $\times$ 1-In surface, a quasi-one-dimensional metallic system, providing an evidence for a metal-insulator transition with one-dimensional charge-density-wave formation in the surface state.

The Si(111)- $\sqrt{3}\times\sqrt{3}$ -Ag surface superstructure ( $\sqrt{3}$ -Ag in short hereafter) is another interesting prototype for surface transport studies since it is well known by its two-dimensional electron-gas (2DEG) system in the surface state which has a free-electron-like parabolic band crossing  $E_F$ .<sup>5-7</sup> In our previous paper,<sup>8</sup> it has been shown that this surface exhibits metallic conduction from room temperature (RT) down to around 150 K, while it changes into an insulating behavior below it. This metal-to-insulator transition in transport is tentatively attributed to strong localization of the surface-state carriers due to random potential, with enhancement by so-called electron standing waves created around inevitable defects on the surface; a periodic potential modulation with a periodicity of a half of the Fermi wavelength enhances the carrier localization. In the present paper, we intend to provide experimental data supporting this idea by intentionally introducing defects on this surface by depositing tiny amounts of additional Au atoms on the  $\sqrt{3}$ -Ag; such defects are expected to enhance the carrier scattering and localization. The metal-insulator transition in conductivity of the pristine  $\sqrt{3}$ -Ag surface was also reported by another group,<sup>9</sup> though the interpretation of the results was different from the carrier localization.

Using macroscopic four-point-probe (4PP) methods in which the probe separation is several millimeters, it has been

found that depositing tiny amounts of monovalent metal atoms, i.e., alkali metals (K, Rb, and Cs) and noble metals (Ag, Au, and Cu) onto the  $\sqrt{3}$ -Ag surface, makes the surface conductance increase significantly.<sup>10</sup> It was discovered later by angle-resolved photoemission spectroscopy (ARPES) that the monovalent adsorbates dope electrons to the surface-state band of the  $\sqrt{3}$ -Ag substrate, shifting the 2DEG band downward below  $E_F$  and thus increasing the nearly free-electron density.<sup>11,12</sup> As a result, the surface conductance increases accordingly with the adsorbate coverage until it became a superstructure, which has a periodicity of  $\sqrt{21}\times\sqrt{21}$  forms at  $\sim 0.14$  monolayer (ML) coverage. Previous scanning tunneling microscopy (STM) studies have shown that at different coverages of the monovalent adatoms, the adsorbate arrangement on the  $\sqrt{3}$ -Ag surface is quite different depending on the adsorbate species and coverage and the substrate temperature.<sup>13</sup> At very low coverage (0.01–0.02 ML) and at low temperature (LT) ( $\sim 135$  K), the adsorbates sit on identical adsorption sites of the  $\sqrt{3}$ -Ag surface, but without long-range order, which induces random attractive potential to the 2DEG. As a result, it makes the 2DEG band split into two;<sup>14</sup> an adatom-induced impurity band and the 2DEG band are hybridized with each other. As the coverage increases, the adsorbates aggregate to form the  $\sqrt{21}\times\sqrt{21}$  superstructures that have quite small domains compared to the  $\sqrt{3}$ -Ag substrate.<sup>15,16</sup> Therefore, the electronic transport behavior is expected to be different at different phases of adsorbates as the coverage changes.

In this paper, by measuring the temperature dependence (110–300 K) of the surface conductance of Au-adsorbed  $\sqrt{3}$ -Ag surface with different Au coverages, we have investigated the dominant mechanism of carrier transport. Before the Au deposition, the surface conductance of pristine  $\sqrt{3}$ -Ag increases as the temperature decreases, indicating a metallic character in which the carriers are mainly scattered by the lattice vibration. However, after small amounts of Au atoms are deposited, nonmetallic transport behavior is observed in the temperature dependence of the surface conductance, although the Au/ $\sqrt{3}$ -Ag systems have shown metallic bands in the previous ARPES studies. Therefore, the nonmetallic transport should be attributed to localization of the surface-state electrons due to random potential induced by the Au adsorbates.

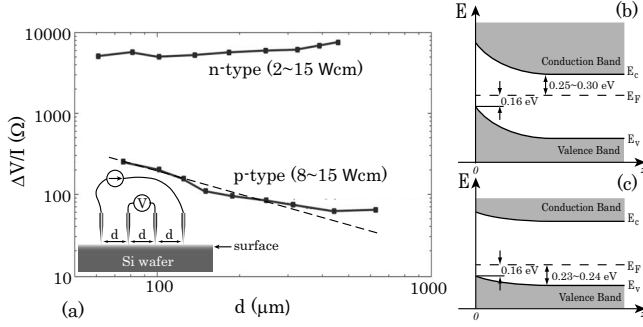


FIG. 1. (a)  $\mu$ 4PP resistance  $R$  of the pristine  $\sqrt{3}$ -Ag surface as a function of probe separation  $d$ , measured on  $n$ - and  $p$ -type Si wafers at RT. A broken line indicates a relation  $R \propto 1/d$ . The inset illustrates the arrangement of four-probes aligned on a sample surface with an equal separation  $d$  in the order of micrometer; (b) and (c) are schematic illustrations of the band bending in the SCL beneath the pristine  $\sqrt{3}$ -Ag surfaces that are formed on  $n$ - and  $p$ -type Si wafers, respectively.

## II. EXPERIMENT

Experiments were performed in an ultrahigh vacuum (UHV) chamber equipped with a setup of micro-four-point-probe ( $\mu$ 4PP) measurement and reflection-high-energy electron-diffraction (RHEED) systems. Details about the home-made  $\mu$ 4PP apparatus are described elsewhere.<sup>4,17</sup> The point of the  $\mu$ 4PP method is that by shrinking the probe separation down to the order of micrometer, the sensitivity to surface is greatly improved in conductivity measurements. In this paper, the probe separation was set to be 20  $\mu\text{m}$  for practical convenience, which was much smaller than the sample size ( $2 \times 15 \times 0.5 \text{ mm}^3$ ). Therefore, the sample can be regarded as infinitely large lateral. The sample and probe were cooled down by thermal conduction from a liquid- $\text{N}_2$  vessel in the UHV chamber.

The RHEED system was used to monitor the surface structures of sample, a P-doped  $n$ -type Si(111) wafer with resistivity of 2–15  $\Omega \text{ cm}$  at RT. After outgassing at  $\sim 400^\circ \text{C}$  overnight, the Si wafer was flashed at  $1250^\circ \text{C}$  several times by direct current heating to obtain a clean Si(111)- $7 \times 7$  surface. The  $\sqrt{3}$ -Ag surface was prepared at a substrate temperature of  $450^\circ \text{C}$  by depositing Ag atoms of about 1 ML. Au atoms were evaporated onto the  $\sqrt{3}$ -Ag surface after cooling the wafer down to RT. A AuFe/chromel thermocouple was fixed very close to the Si wafer (3 mm away from one side of the Si wafer) for measuring the sample temperature below RT.

The experiments of ARPES were performed in another UHV chamber of which details are described elsewhere.<sup>7,13,18</sup> The light source was He I with photon energy of 21.2 eV, and the analyzer was Scienta SES-100. Energy resolution in the ARPES experiment is  $\sim 35 \text{ meV}$ .

## III. RESULTS AND DISCUSSION

### A. Comparison of resistances

The inset of Fig. 1(a) shows the arrangement of the four-probes aligned on a sample surface with equal spacing  $d$ .

Current  $I$  was injected into the sample from the outer pair of probes, and the voltage drop  $\Delta V$  was detected by the inner pair. Thus, we could obtain the four-point-probe resistance from the gradient of current-voltage curves,  $R = d(\Delta V)/dI$ .

In a simplified three-layer model, the injected current can flow through three channels in parallel: *surface states* on the topmost atomic layers, bulk states in the *surface space-charge layer* (SCL) just beneath the surface, and bulk states in the *interior of substrate*.<sup>2,19</sup> By making the probe spacing as small as the thickness of the SCL or less than it, the last channel can be reduced significantly, as demonstrated by previous experimental results.<sup>19</sup> One can roughly evaluate the contribution of bulk channel to the  $\mu$ 4PP measurement by investigating the dependence of the 4PP resistance on the probe spacing.<sup>19</sup> If the current penetrates deeply into the bulk, the system can be simplified with a homogeneous semi-infinite three-dimensional (3D) resistive material, for which the measured 4PP resistance  $R$  should be inversely proportional to the probe spacing  $d$ ,

$$R = \frac{\rho}{2\pi d}, \quad (1)$$

where  $\rho$  is the bulk resistivity.<sup>19</sup> In contrast, if the current flows only through the surface layer (surface state and SCL), the sample should be regarded as an infinite 2D sheet, for which  $R$  is independent of  $d$ ,

$$R = \frac{\ln 2}{2\pi} R_s, \quad (2)$$

where  $R_s$  is the sheet resistivity.<sup>19</sup>

Figure 1(a) shows the probe-spacing dependence of 4PP resistance measured by four-tip STM at RT<sup>20,21</sup> on two kinds of pristine  $\sqrt{3}$ -Ag surfaces, one of which is formed on a  $n$ -type Si wafer, while the other on a  $p$ -type one. On the  $p$ -type wafer the resistance decreases as the probe separation is increased, while on the  $n$ -type one it changes little, in agreement with Eqs. (1) and (2), respectively. This result can be easily understood if we notice that the SCLs beneath the  $\sqrt{3}$ -Ag surface formed on  $n$ - and  $p$ -type Si wafers are different. The band bendings in the SCL in the respective wafers are schematically illustrated in Figs. 1(b) and 1(c), respectively, based on the fact that  $E_F$  is pinned at 0.16 eV above the valence-band maximum at the  $\sqrt{3}$ -Ag surface.<sup>11</sup> This surface Fermi-level position is determined by photoemission spectroscopy. In the  $n$ -type Si wafer, the SCL is a weak inversion layer [Fig. 1(b)], which induces a  $p$ - $n$  junction between the surface and the interior of the Si crystal so that the current is confined in the region very close to the surface only, meaning a two-dimensional (2D) current distribution. In the  $p$ -type Si wafer, in contrast, the SCL is an accumulation layer [Fig. 1(c)] where the carrier density is even larger than that in the deep bulk, so that the current penetrates deep into the bulk, meaning three-dimensional current distribution. Based on the experimental results in Fig. 1(a), we conclude that in the measured  $\mu$ 4PP resistance of the  $\sqrt{3}$ -Ag surface formed on the  $n$ -type Si wafer, the bulk contribution is negligible, while the  $p$ -type wafer shows a bulk property. This is also shown by the resistance value itself; the mea-

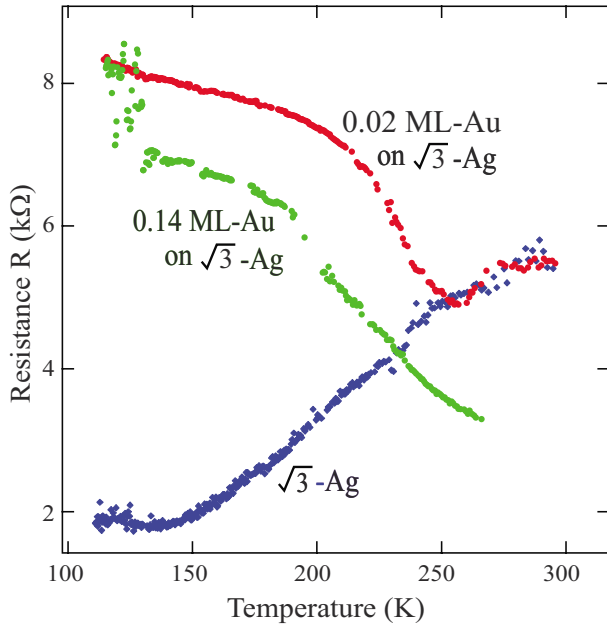


FIG. 2. (Color online) Temperature dependences of  $\mu$ 4PP resistance of three samples: the pristine Si(111)- $\sqrt{3} \times \sqrt{3}$ -Ag and the same surfaces with 0.02 and 0.14 ML of additional Au atoms deposited on it.

measured values of resistance for the  $p$ -type wafer are consistent with the bulk resistivity of the wafer, while those of the  $n$ -type wafer are nearly 2 orders of magnitudes higher than that expected from the bulk resistivity. This is the reason why we choose a  $n$ -type Si wafer as the substrate for studying the sheet conductance through the surface states in this paper.

On the  $n$ -type Si wafer, after submonolayer of Au atoms is deposited onto the  $\sqrt{3}$ -Ag surface, it is known that the band bending in the SCL becomes moderate so that the SCL becomes a depletion layer due to an upward shift of the surface  $E_F$ .<sup>11</sup> Accordingly, the carrier (hole) density in the SCL decreases. Therefore, the interior bulk contribution to the  $\mu$ 4PP measurement is neglected not only in the pristine  $\sqrt{3}$ -Ag surface but also in the Au-adsorbed ones. In this case, the measured resistance  $R$  can be converted into a sheet conductivity  $\sigma_{\text{meas}}$  according to Eq. (2),

$$\sigma_{\text{meas}} = \frac{\ln 2}{2\pi R}. \quad (3)$$

Because there are two channels for the current to flow through, the measured  $\sigma_{\text{meas}}$  consists of two parts, one is from the surface states  $\sigma_{\text{SS}}$  and the other from SCL  $\sigma_{\text{SCL}}$ ,  $\sigma_{\text{meas}} = \sigma_{\text{SS}} + \sigma_{\text{SCL}}$ , though  $\sigma_{\text{SS}}$  dominates over  $\sigma_{\text{SCL}}$  for the reason mentioned in Secs. III B–III D.

Figure 2 shows the temperature dependences of the measured 4PP resistance of three types of samples: the pristine  $\sqrt{3}$ -Ag, 0.02 ML Au-adsorbed  $\sqrt{3}$ -Ag, and 0.14 ML Au-adsorbed  $\sqrt{3}$ -Ag (which is the  $\sqrt{21} \times \sqrt{21}$  surfaces). The resistance decreased monotonously from RT to about 140 K for the pristine  $\sqrt{3}$ -Ag surface, while the temperature dependence of resistance changed dramatically just by depositing

the submonolayer Au atoms on it. The resistance began to rise by cooling below approximately 250 K for the 0.02 ML Au-adsorbed surface. The 0.14 ML Au-adsorbed surface showed a monotonous increase in resistance by cooling. It was a surprise that such a tiny amount of Au adsorption changed the character of surface conduction so drastically. In Secs. III B–III D, we discuss the characters and transport mechanisms of the respective samples in detail.

### B. Pristine $\sqrt{3}$ -Ag surface: Metallic conduction

Figure 3(a) shows the sheet conductivity  $\sigma_{\text{meas}}$  obtained from the measured  $\mu$ 4PP resistance  $R$  for the pristine  $\sqrt{3}$ -Ag surface shown in Fig. 2. All of the measured  $I$ - $V$  curves kept linear around zero current from RT to the lowest temperature; some of which are displayed in the inset of Fig. 3(a).  $\sigma_{\text{meas}}$  increases with lowering the temperature down to  $\sim 140$  K, which means a metallic character. Below 140 K, the conductivity turns to decrease with cooling, which corresponds to a metal-insulator transition reported previously.<sup>8</sup>

In order to elucidate  $\sigma_{\text{SS}}$ , we have evaluated  $\sigma_{\text{SCL}}$  by a calculation as a function of temperature  $T$ , which is plotted in Fig. 3(a) with a solid line. In the calculation, since the  $E_F$  positions at the surface and in the deep bulk are known, we obtained, by using a well-established method by solving the Poisson's equation,<sup>22</sup> the band bending and the resulting excess carrier concentration at the SCL which is  $T$  dependent through the Fermi-Dirac distribution function. The  $T$  dependence of the carrier mobility in the SCL is also involved in the calculation.<sup>22</sup> We see from Fig. 3(a) that  $\sigma_{\text{SCL}}$  decreases with lowering  $T$ , showing a typical semiconducting behavior. However, the measured  $\sigma_{\text{meas}}$  has an opposite tendency, a metallic character. Thus we can safely claim that the main feature in the  $T$  dependence of  $\sigma_{\text{meas}}$  is dominated by  $\sigma_{\text{SS}}$ .

Since the pristine  $\sqrt{3}$ -Ag surface has, as mentioned before, a 2D nearly free-electron band crossing  $E_F$ ,  $\sigma_{\text{SS}}$  can be calculated by the Boltzmann equation using the band parameters obtained by ARPES,<sup>18</sup>

$$\sigma_{\text{SS}} = \frac{e^2}{2} (\tau v_F) v_F D_F, \quad (4)$$

where  $\tau$  is the carrier relaxation time,  $v_F$  the Fermi velocity, and  $D_F$  the 2D density of states at  $E_F$ . In the Boltzmann picture, thus, the electron transport is governed by the number density and velocity of 2D Fermi electrons, both of which are almost independent of  $T$  in the case of a metallic system as long as there is no temperature-induced phase transition. Therefore, the  $T$  dependence of conductivity originates from the relaxation time  $\tau$  only ( $\tau$  is assumed to be independent of the wave vector  $\mathbf{k}$  for simplicity.<sup>23</sup>)

Usually in a metallic system, the carriers are mainly scattered by phonons as long as the impurity concentration is not too high and the temperature is not very low. In this case, at temperature higher than the Debye temperature,<sup>24</sup>  $\tau$  is inversely proportional to  $T$ . Since the Debye temperature for the Ag layer of the  $\sqrt{3}$ -Ag surface is measured to be 140 K by positron diffraction experiments,<sup>25</sup> from Eq. (4) we can expect  $\sigma_{\text{SS}} \propto T^{-1}$ .

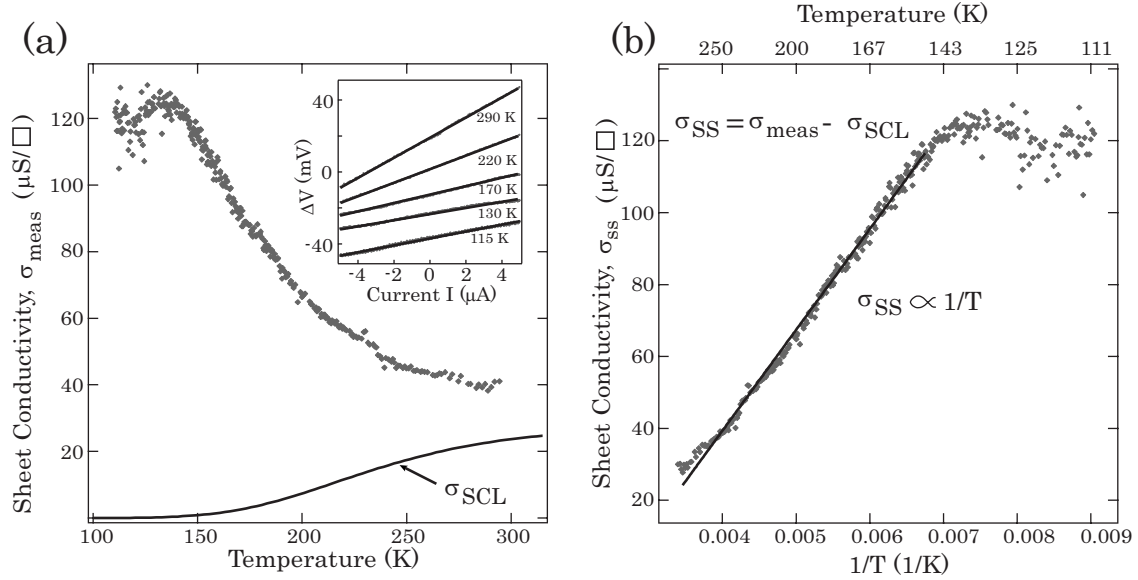


FIG. 3. (a) Measured sheet conductivity of the pristine  $\sqrt{3}$ -Ag surface and theoretically calculated SCL contribution (solid line),  $\sigma_{SCL}$ , as a function of temperature. The inset presents some raw data of the  $I$ - $V$  curves taken at indicated temperatures. The curves are shifted up or down for better display. (b) The surface-state sheet conductivity  $\sigma_{SS}$  of the pristine  $\sqrt{3}$ -Ag surface as a function of  $T^{-1}$ . The straight line is a fitted one by  $\sigma_{meas} \propto 1/T$ .

To confirm it, we replot  $\sigma_{SS}(=\sigma_{meas}-\sigma_{SCL})$  as a function of  $T^{-1}$  in Fig. 3(b). As expected,  $\sigma_{SS}$  is proportional to  $T^{-1}$  from RT to  $\sim 150$  K. Therefore, we conclude that the dominant scattering mechanism for the transport electrons in the  $\sqrt{3}$ -Ag surface state is an electron-phonon interaction, which, in fact, has been confirmed also by recent ARPES studies.<sup>8</sup>

It is noticed in Fig. 3 that at temperature lower than  $\sim 140$  K,  $\sigma_{SS}$  does not increase anymore but starts to decrease, behaving like a semiconductor. Because the ARPES study does not find any change in the electronic band structure of the pristine  $\sqrt{3}$ -Ag surface during cooling, we do not think that this is a metal-insulator phase transition with an energy-gap opening at  $E_F$  around this temperature. Instead, we think it is due to interference of conduction electrons scattered by inevitable defects such as impurities/point defects and atomic steps on the crystal surface. The details are described in Ref. 8. At higher temperature, the mean-free path dominated by phonon scattering is short, so that the interference effect is not so significant, while at lower temperature ( $\leq 140$  K in the present case), due to elongation of the coherence length of the surface-state electrons, the Friedel oscillation around defects grows so that the carriers at  $E_F$  are scattered and localized by the periodic potential variation due to the Friedel oscillation. As a result, the temperature dependence of  $\sigma_{SS}$  changes from a metallic behavior to a semiconducting behavior due to the localization effect. As the experimental data in the temperature range for the semiconducting behavior are limited, we discuss it in more detail below, by intentionally introducing some Au adatoms, which act as defects inducing the localization, onto the clean  $\sqrt{3}$ -Ag surface.

**C. 2D Au nanoclusters on  $\sqrt{3}$ -Ag surface: Carrier localization**

Figure 4 shows the  $T$  dependence of the sheet conductivity converted from the data in Fig. 2 by Eq. (3). Based on our

photoemission spectroscopy (PES) studies as well as previous studies,<sup>10</sup> after depositing 0.02 ML of Au atoms on the  $\sqrt{3}$ -Ag surface, the  $E_F$  position measured from  $E_V$  changes from 0.16 to 0.28 eV [see Fig. 1(b)]. Therefore, the Au adatoms make the band bending in the SCL moderate so as to

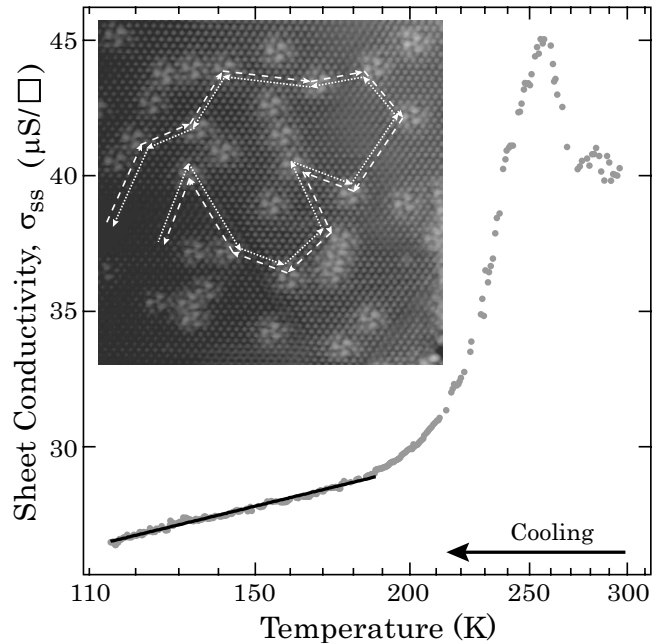


FIG. 4.  $T$  dependence of the sheet conductivity of the  $\sqrt{3}$ -Ag surface with 0.02 ML Au adsorption calculated from the 4PP resistance shown in Fig. 2 by Eq. (3). The horizontal axis is  $T$  on a logarithmic scale. The straight line is a fitted result by Eq. (5). The inset is a typical LT-STM image of the Au-nanocluster phase on the  $\sqrt{3}$ -Ag surface. Transport electron paths are drawn with broken lines to show schematically the enhancement of backscattering process (Ref. 26).

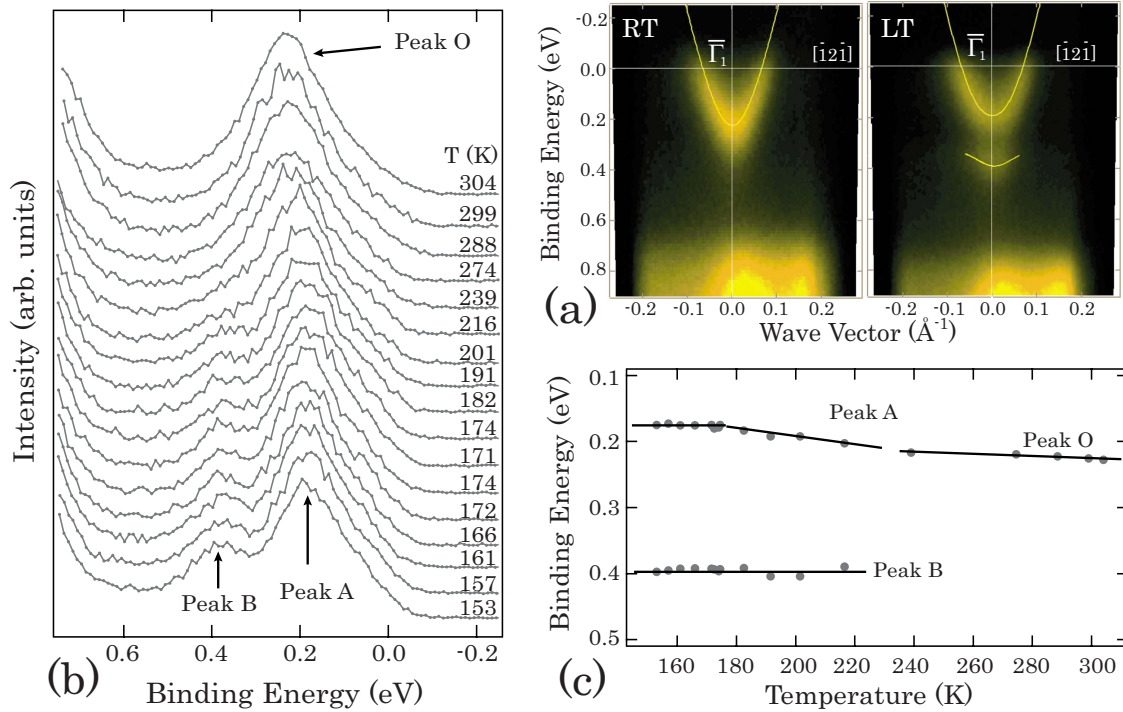


FIG. 5. (Color online) (a) 2DEG band dispersion of the  $\sqrt{3}$ -Ag surface on which  $\sim 0.01$  ML of Au atoms was deposited taken at RT (left) and 135 K (right). After cooling, the 2DEG band was split into two (Ref. 14). (b) Photoemission spectra of the sample surface used in (a), taken at various temperature from RT to  $\sim 150$  K. The spectra were recorded at  $\bar{\Gamma}_2$  point on the  $[10\bar{1}]$  direction. Peak O at RT is split into two: peak A and peak B at LT. (c) Temperature dependence of the binding energy of peak O, peak A, and peak B; Lines are drawn for eye guide.

reduce the SCL contribution to the measured conductance.  $\sigma_{\text{SCL}}$  for this surface is calculated to be  $0.2 \mu\text{S}$  at RT, which is much smaller than the measured sheet conductivity,  $\sigma_{\text{meas}}$ , so we conclude that  $\sigma_{\text{meas}}$  is approximately equal to the sheet conductivity only through the metallic surface-state band of the Au-adsorbed  $\sqrt{3}$ -Ag surface:  $\sigma_{\text{meas}} \simeq \sigma_{\text{SS}}$ .

The  $T$  dependence of  $\sigma$  is completely different from that of the pristine  $\sqrt{3}$ -Ag surface. From RT to  $\sim 250$  K, we see from Fig. 4 that the sheet conductance increases as the temperature decreases. It is a metallic behavior as expected since the surface has a metallic 2DEG band at  $E_F$  according to ARPES studies. However, from  $\sim 250$  to  $\sim 115$  K, the sheet conductance decreases with lowering temperature, showing a clear semiconducting behavior. Above  $\sim 190$  K,  $\sigma$  decreases very rapidly with cooling, while below this temperature, the decrease becomes moderate.

Since the electronic transport is governed by the electrons near  $E_F$  as indicated by Eq. (4), studying the changes in DOS at  $E_F$  during cooling is very important for understanding the behavior of the transport in Fig. 4. Our recent studies<sup>14</sup> revealed that Au adsorbates of 0.02 ML on the  $\sqrt{3}$ -Ag surface kept migrating freely at RT, while they were frozen on identical adsorption sites at low temperatures to form Au nanoclusters. These Au nanoclusters induce resonant virtual bound states around themselves that overlap with each other, forming an impuritylike band at low temperatures. This band hybridizes with the 2DEG surface-state band of the  $\sqrt{3}$ -Ag substrate and makes it split into two [see Fig. 5(a)].<sup>14</sup> During cooling, therefore, the DOS as well as other properties such

as Fermi velocity and effective mass of the electrons at  $E_F$  are altered, so that the change in sheet conductance is very complicated according to the Boltzmann picture under a nearly free-electron model [see Eq. (4)].

To understand the behavior of the  $T$  dependence of surface-state sheet conductance  $\sigma_{\text{SS}}$ , we investigated using ARPES the detailed changes in the 2DEG band during cooling, which are shown in Fig. 5(b). The sample surface used for the present ARPES experiment is  $\sqrt{3}$ -Ag with Au coverage of 0.01 ML, but we believe that the quantitative conclusion made from it should be also valid for the sample surface at Au coverage of 0.02 ML used in the  $\mu\text{4PP}$  conductivity measurements. It is seen from Fig. 5(b) that from 304 to 239 K, there is only a strong peak (peak O) located at a binding energy around 0.2 eV, while from 216 to 153 K, there are two peaks being recognized, peak A and peak B, indicated by two arrows. As mentioned above, the mechanism for the band splitting induced by cooling is the hybridization of the Au-nanocluster-induced resonance states with the 2DEG bands.<sup>14</sup> Here we concentrate on the changes in binding energy of the peaks with temperature. In other words, we are trying to find out the relation between the splitting of the band in Fig. 5 and the change in the sheet conductance in Fig. 4. For this purpose, Lorentzian function with a background of baseline was employed to reproduce the spectra shown in Fig. 5(b). The spectra from 304 to 239 K were fitted with only one peak while the others with two peaks. The fitted binding energy of each peak is plotted in Fig. 5(c) as a function of temperature.

It is seen in Fig. 5(c) that the changes in binding energy during cooling can be divided into three regions: the first one is from RT to  $\sim 240$  K where there is only peak O at the binding energy  $\sim 0.22$  eV; the second region is from  $\sim 240$  to  $\sim 180$  K where peak A shifts gradually toward  $E_F$ ; and the last region is below  $\sim 180$  K where peak A keeps a binding energy of  $\sim 0.18$  eV. It is very interesting to see that the  $T$  dependence of  $\sigma_{SS}$  in Fig. 4 can also be divided into three temperature regions: from RT to  $\sim 250$  K,  $\sigma$  increases as temperature decreases; from  $\sim 250$  to  $\sim 190$  K,  $\sigma$  decreases dramatically with cooling; and below  $\sim 190$  K,  $\sigma$  decreases moderately. This indicates that  $T$  dependence of  $\sigma$  has a strong correlation with that of the 2DEG band in Fig. 5.

From RT to  $\sim 240$  K, the band does not split because the Au atoms are in a 2D adatom gas (2DAG) state,<sup>14</sup> namely, the electronic band structure has not been altered yet, so that  $D_F$  and  $v_F$ , both of which are decisive factors to the conductance, should not change yet. Therefore, the sheet conductance increases with decreasing temperature due to reduction in lattice vibration, basically like the behavior of  $\sigma_{SS}$  in Fig. 3(b), a typical behavior in a 2D metallic system.

From  $\sim 240$  to  $\sim 180$  K, the 2DEG band splits into two, namely, peak O splits into peak A and peak B. It is seen in Fig. 5(c) that peak A shifts gradually toward  $E_F$ , while the energy shift of peak B is negligible. Such a shift of peak A is an evidence that the 2DEG band keeps changing during cooling within this temperature region. Because the density of electrons does not change, namely, the Fermi wave vector does not change, the Fermi velocity decreases while the effective mass increases gradually due to the upward shift of peak A. As a result, the surface-state sheet conductance  $\sigma$  decreases with temperature dramatically, as shown in Fig. 4. However, it is too complicated to quantitatively depict the decreasing procedure of the sheet conductance at this temperature region, since the details of the change in  $v_F$  and  $D_F$  are unknown (we do not have the band dispersion diagram at each temperature).

Below  $\sim 180$  K, we see from Fig. 5(c) that peak A does not shift anymore. In the same temperature range, the decrease in sheet conductance with cooling becomes moderate. No more shift of peak A means that the intrinsic properties of conduction electrons such as  $v_F$  and  $D_F$  may not change anymore. Therefore, it is possible to discuss the dominant scattering mechanism in this temperature region.

In Fig. 4, we set the horizontal axis of temperature on a logarithmic scale. It is interesting to find that  $\sigma$  is proportional to  $\ln T$  below  $\sim 180$  K, which is exactly an expected result of a weak localization effect induced by random potential. Combining with LT-STM image shown in the inset of Fig. 4, the weak localization effect can be understood in terms of an enhancement of backscattering of carriers.<sup>26</sup>

However, in addition to the weak localization effect, Altshuler *et al.*<sup>27</sup> and Fukuyama<sup>28</sup> pointed out that similar logarithmic behavior in the temperature dependence of sheet conductance is expected if the mutual Coulomb interaction of the conduction electrons is considered. The predicted conductivity  $\sigma$  for a 2D electron gas in the metallic nonactivated range has the form<sup>29,30</sup>

$$\sigma(T) = \sigma(T_0) + \frac{Ce^2}{2\pi^2\hbar} \ln \frac{T}{T_0}, \quad (5)$$

where

$$C = \alpha p + (1 - F). \quad (6)$$

The first term in Eq. (6) is from the weak localization effect where  $\alpha$  is a constant prefactor,  $\alpha=1$  for spin-independent scattering (the present case) and  $\alpha=1/2$  for strong spin-flip scattering.<sup>31</sup> The index  $p$  depends on the dominant inelastic collision mechanism, and the temperature dependence of the inelastic-scattering time  $\tau_{in}$  is expressed as  $\tau_{in} \propto T^{-p}$ . In case that the dominant inelastic scattering is the lattice vibration,  $p=1$  is expected.

The second term in Eq. (6) is from the electron-electron interaction where the Hartree parameter  $F$  depends on the ratio of the Fermi wavelength to the screening length.  $F$  approaches one for strong screening and zero for weak screening.<sup>27</sup> In the extreme condition,  $\tau^{-1}=0$  and considering only electrons at  $E_F$ ,  $F$  can be expressed in a simplified form,

$$F = \int_0^{2\pi} \frac{d\theta/2\pi}{1 + (2k_F/K)\sin(\theta/2)}, \quad (7)$$

determined from the angular average of the statically screened Coulomb interaction. Here  $K$  is the 2D electron screening constant, given in a nearly free-electron model by

$$K = \frac{m^* e^2}{2\pi\epsilon\hbar^2}, \quad (8)$$

where  $\epsilon$  is the dielectric constant of the surrounding materials.

Ono *et al.*<sup>32</sup> found the value of  $K$  to be  $0.064 \text{ \AA}^{-1}$  for the  $\sqrt{3}$ -Ag surface by taking  $\epsilon$  as an average of the vacuum and silicon substrate. Since  $k_F$  is determined by PES (Ref. 14), the Hartree parameter  $F$  is calculated by Eq. (7) to be 0.4. This value is not small enough to be neglected, so that contribution of electron-electron interaction to the logarithmic behavior in the temperature dependence of sheet conductance may not be negligible according to this simplest model. One way to make this issue clearer is to perform electrical transport measurements in a magnetic field, which may reduce the enhancement of backscattering induced by random potentials. In the present case, we believe that the weak localization effect is dominated by the random potential created by Au nanoclusters, since the logarithmic behavior of the sheet conductance is relevant to the band splitting that is induced by the random potentials.

Using Eq. (5), we fit the sheet conductance as a function of temperature below 180 K, as shown in Fig. 4, and obtain the parameters  $C=0.87 \pm 0.01$  and  $\sigma(T_0=1 \text{ K})=4.5 \pm 0.2 \text{ } \mu\text{S}$ . The value of coefficient  $C$  obtained here is reasonable compared to the previously reported values, for example, 0.75 found in a thin film<sup>33</sup> and 0.71–0.90 found in an inversion layer in a semiconductor.<sup>30</sup>

It is noted that the temperature range for observing the effect of weak localization is quite high in the present case compared to most of the previously reported experiments performed on thin films and inversion layers, where the tem-

perature range is from several kelvins to several tens of kelvins. We think that it is because the 2DEG in a surface-state band that locates in a band gap of the bulk band structure is more sensitive to the random potentials induced by adsorbates at the surface. Actually, it is not so surprising to find a weak localization effect at a temperature higher than 100 K. Markiewicz and Harris<sup>33</sup> even found a logarithmic temperature dependence continuing up to RT in a film with only 1 ML thick.

#### D. $\sqrt{21}$ -Au superstructure: 2D granular metal

When the coverage of Au adatoms on the  $\sqrt{3}$ -Ag surface reaches 0.14 ML, the randomly dispersed Au nanoclusters aggregate into a  $\sqrt{21}$ -Au superstructure, which is also a 2DEG system as revealed by previous ARPES experiments.<sup>11,12</sup> This 2DEG system was expected to exhibit a metallic behavior in the electronic transport, since there are no random potentials to the conduction electrons due to the Au nanoclusters described in Sec. III C anymore. However, our  $\mu$ 4PP measurements show an opposite result that the  $\sqrt{21}$ -Au surface displays a semiconducting behavior in the temperature dependence of resistance (Fig. 2). We attribute it partly to the deficiency of the  $\sqrt{21}$ -Au superstructure such as high-density domain boundaries that may be potential barriers for charge carriers.

Because the SCL underneath the  $\sqrt{21}$ -Au surface on the  $n$ -type Si wafer is a depletion layer where the carrier density is extremely low,<sup>11</sup> we need to consider the transport contributions neither from the interior of bulk region nor even from the SCL region. Therefore, the measured resistance in Fig. 2 can be converted into the sheet conductance  $\sigma_{SS}$  by Eq. (4), and its temperature dependence is displayed in Fig. 6. The measured sheet conductance is approximately equal to that through the layer of the  $\sqrt{21}$ -Au superstructure, i.e., the surface-state conductivity  $\sigma_{SS}$ .

The sheet conductance of the  $\sqrt{21}$ -Au surface at approximately RT is larger than that of the  $\sqrt{3}$ -Ag surface shown in Fig. 3(a), which is consistent with the previous reports that electron doping from Au adatoms to the substrate increases the sheet conductance.<sup>34,35</sup> However, it is obvious in Fig. 6 that the sheet conductance has a semiconducting behavior in the temperature dependence in spite of the metallic 2DEG band that the surface has. This result indicates that the electron scattering in the  $\sqrt{21}$ -Au surface is so complicated that cannot be explained well only by a simple band theory.

One possible reason for such an unexpected semiconducting behavior in the electronic transport of the  $\sqrt{21}$ -Au surface is the high-density domain boundaries. Because the  $\sqrt{21}$ -Au superstructure is formed on the  $\sqrt{3}$ -Ag substrate without heat treatment, any defects on the pristine substrate would affect the aggregation of Au nanoclusters, preventing them from growing into a large domain of  $\sqrt{21}$ -Au surface. As a result, the  $\sqrt{21}$ -Au surface is divided into much smaller domains compared to the pristine  $\sqrt{3}$ -Ag substrate. The inset of Fig. 6 shows a STM image displaying such small domains in the  $\sqrt{21}$ -Au surface. The domain boundaries act as potential barriers for conduction electrons. As long as the applied bias between two adjacent domains is not too high, thermal acti-

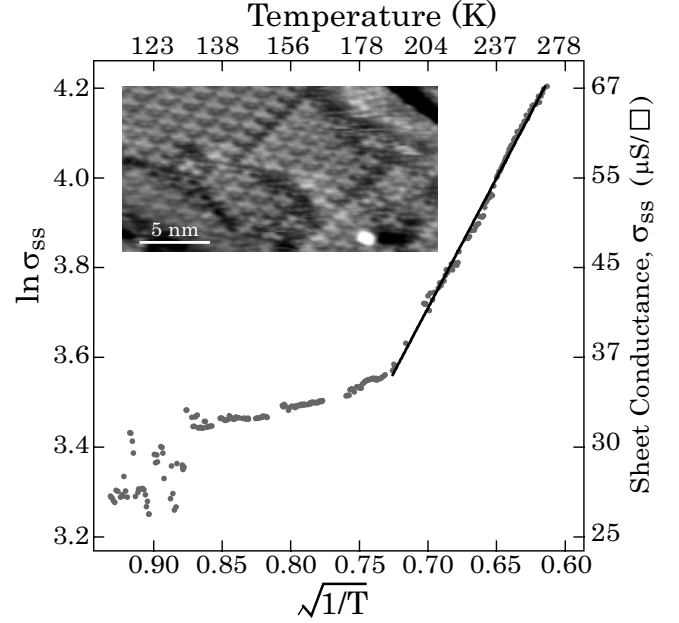


FIG. 6.  $T$  dependence of the sheet conductivity of the surface state  $\sigma_{SS}$  of the  $\sqrt{21}$ -Au surface formed by adsorption of  $\sim 0.14$  ML of Au on the  $\sqrt{3}$ -Ag calculated from the  $\mu$ 4PP resistance shown in Fig. 2 by using Eq. (4). The left and bottom axes are on the scale of  $\ln \sigma$  and  $\sqrt{1/T}$ , respectively. The values of  $\sigma$  and  $T$  are shown on the right and top axes, respectively. The inset is an STM image taken on the  $\sqrt{21}$ -Au surface.

vation is the main mechanism responsible for charge-carrier generation. Therefore, the sheet conductance decreases with temperature. This picture is actually an analogy to that of granular metals in which metallic grains touch each other in a manner that electrons transporting between two neighboring grains have to overcome a potential barrier located between them.

According to the theoretical analysis of Abeles *et al.*,<sup>36</sup> the temperature dependence of the conductance through granular-metal films in low electric field is expressed as

$$\sigma = \sigma_0 e^{-2\sqrt{C/k_B T}}, \quad (9)$$

where  $C$  is a constant concerning the barrier height and  $\sigma_0$  is also a constant independent of temperature. We rewrite Eq. (9) as

$$\ln \sigma = \ln \sigma_0 - 2\sqrt{C/k_B} \sqrt{1/T}. \quad (10)$$

In Fig. 6, we plotted  $\ln \sigma$  as a function of  $\sqrt{1/T}$ . It is seen that in the temperature range from  $\sim 270$  to  $\sim 180$  K,  $\ln \sigma$  is approximately proportional to  $\sqrt{1/T}$ , exactly as the granular-metal theory predicts. By fitting Eq. (10) to the data in Fig. 6, we obtained the values of the coefficients,  $\sigma_0 = 2.6 \pm 0.4$  mS and  $C = 0.076 \pm 0.008$  eV.

In essence, the granular-metal theory depicts a kind of hopping conduction<sup>37,38</sup> that has been widely studied in disordered systems. In the present case, electrons are localized in the respective domains that are separated from each other by the domain boundaries, in analogy to the granular metals. At a low electrical field, electrons hop from one domain to

the other with help of thermal activation. Thus, the activated transport behavior of the sheet conductance at temperature higher than  $\sim 180$  K is roughly explained by the granular-metal theory.

However, the temperature dependence of the sheet conductance deviates from the prediction of the granular-metal theory at  $T < 180$  K, as seen in Fig. 6. The decrease in the sheet conductance becomes moderate at this temperature region, indicating a transition of dominant transport mechanism at  $T \sim 180$  K. This unexpected behavior is not understood well yet. Considering that the Au adatoms transit from 2D adatom gas phase to nanocluster phase also around  $T \sim 180$  K, we speculate that such an “electronic transport” transition concerns the transition of the Au adatom state, although the correlation between them is not known yet.

Actually, during the STM observations on the  $\sqrt{21}$ -Au superstructure, there was always much deficiency such as domain boundaries, isolated Au nanoclusters, and inevitable steps on the substrate surface. It is such defects in the  $\sqrt{21}$ -Au superstructure that makes the transport mechanism complicated.

#### IV. SUMMARY

The  $\mu$ 4PP conductance measurements were performed on the Au-adsorbed  $\sqrt{3}$ -Ag surface as well as on the pristine  $\sqrt{3}$ -Ag surface itself to investigate the electronic transport through the metallic surface state. Because of the depletion area in the SCL beneath the surface, the current did not flow through the bulk of the  $n$ -type Si substrate, and it helps us to make the measurements very surface sensitive. As a result, the measured sheet conductivity consists of the contributions only from the surface state and the SCL. In addition, the SCL contribution is subtracted by theoretical calculations so that the surface-state conductivity is obtained from three types of surfaces, all of which have metallic bands as revealed in

previous ARPES studies, but two of them show semiconducting behavior in the temperature dependence of conductivity.

By analyzing the temperature dependence of the sheet conductivity of the surface state in detail, we have discussed the dominant transport mechanism in the three types of metallic surfaces. In the pristine  $\sqrt{3}$ -Ag surface, the surface-state conductivity is inversely proportional to temperature, exhibiting a typical transport behavior expected in a 2D metallic system where the electrons are mainly scattered by lattice vibration. In the Au-nanocluster phase where 0.02 ML of Au atoms is deposited on the  $\sqrt{3}$ -Ag surface, the Au adatoms play a role of scatters to the conduction electrons by producing random potential. After cooled down, the surface-state conduction electrons are weakly localized by the randomly dispersed Au nanoclusters. This leads to a semiconducting and logarithmic temperature dependence of sheet conductance. In the  $\sqrt{21}$ -Au surface that is formed by depositing 0.14 ML of Au atoms on the  $\sqrt{3}$ -Ag surface, the electronic transport exhibits an unexpected semiconducting behavior despite of the metallic 2DEG surface-state band. At temperature higher than  $\sim 180$  K, it is roughly explained by the granular-metal theory, considering that electrons are localized in the isolated and small  $\sqrt{21}$ -Au domains. At lower temperature, however, the temperature dependence of the surface conductance deviates from the interpretation, showing a more moderate decreasing behavior. More studies are required to make a full understanding of the dominant transport mechanism in the  $\sqrt{21}$ -Au surface states.

#### ACKNOWLEDGMENTS

S. Yamazaki is acknowledged for discussions. This work has been supported by a Grant-In-Aid and A3 Foresight Program from the Japan Society for the Promotion of Science.

\*Present address: International Center for Young Scientists, National Institute for Materials Science, 1-1 Namiki, Tsukuba 305-0044, Japan.

†Present address: Institute for Solid State Physics, University of Tokyo, 5-1-5 Kashiwa-no-ha, Kashiwa, Chiba 277-8581, Japan.

<sup>1</sup>P. W. Anderson, *Science* **235**, 1196 (1987).

<sup>2</sup>M. Henzler, in *Surface Physics of Materials I*, edited by J. M. Blakely (Academic, New York, 1975), p. 241.

<sup>3</sup>S. Hasegawa and F. Grey, *Surf. Sci.* **500**, 84 (2002).

<sup>4</sup>T. Tanikawa, I. Matsuda, T. Kanagawa, and S. Hasegawa, *Phys. Rev. Lett.* **93**, 016801 (2004).

<sup>5</sup>H. Aizawa, M. Tsukada, N. Sato, and S. Hasegawa, *Surf. Sci. Lett.* **429**, L509 (1999).

<sup>6</sup>N. Sato, T. Nagao, S. Takeda, and S. Hasegawa, *Phys. Rev. B* **59**, 2035 (1999).

<sup>7</sup>T. Hirahara, I. Matsuda, M. Ueno, and S. Hasegawa, *Surf. Sci.* **563**, 191 (2004).

<sup>8</sup>I. Matsuda, C. Liu, T. Hirahara, M. Ueno, T. Tanikawa, T. Kanagawa, R. Hobara, S. Hasegawa, and K. Kobayashi, *Phys. Rev. Lett.* **99**, 146805 (2007).

<sup>9</sup>J. W. Wells, J. F. Kallehauge, and Ph. Hofmann, *J. Phys.: Condens. Matter* **19**, 176008 (2007).

<sup>10</sup>S. Hasegawa, X. Tong, S. Takeda, N. Sato, and T. Nagao, *Prog. Surf. Sci.* **60**, 89 (1999).

<sup>11</sup>X. Tong, C. S. Jiang, and S. Hasegawa, *Phys. Rev. B* **57**, 9015 (1998).

<sup>12</sup>J. N. Crain, K. N. Altmann, C. Bromberger, and F. J. Himpsel, *Phys. Rev. B* **66**, 205302 (2002).

<sup>13</sup>C. Liu, S. Yamazaki, R. Hobara, I. Matsuda, and S. Hasegawa, *Phys. Rev. B* **71**, 041310(R) (2005).

<sup>14</sup>C. Liu, I. Matsuda, R. Hobara, and S. Hasegawa, *Phys. Rev. Lett.* **96**, 036803 (2006).

<sup>15</sup>J. Nogami, K. J. Wan, and X. F. Lin, *Surf. Sci.* **306**, 81 (1994).

<sup>16</sup>A. Ichimiya, H. Nomura, Y. Horio, T. Sato, T. Sueyoshi, and M. Iwatsuki, *Surf. Rev. Lett.* **1**, 1 (1994).

<sup>17</sup>T. Tanikawa, I. Matsuda, R. Hobara, and S. Hasegawa, *e-J. Surf. Sci. Nanotechnol.* **1**, 50 (2003).

<sup>18</sup>I. Matsuda, T. Hirahara, M. Konishi, C. Liu, H. Morikawa, M. D'angelo, S. Hasegawa, T. Okuda, and T. Kinoshita, *Phys. Rev. B* **71**, 235315 (2005).

- <sup>19</sup>S. Hasegawa, S. Ichiro, F. Tanabe, R. Hobara, T. Kanagawa, T. Tanikawa, I. Matsuda, C. L. Petersen, T. M. Hansen, P. Boggild, and F. Grey, *Surf. Rev. Lett.* **10**, 963 (2003).
- <sup>20</sup>I. Shiraki, F. Tanabe, R. Hobara, T. Nagao, and S. Hasegawa, *Surf. Sci.* **493**, 633 (2001).
- <sup>21</sup>S. Hasegawa, I. Shiraki, F. Tanabe, and R. Hobara, *Curr. Appl. Phys.* **2**, 465 (2002).
- <sup>22</sup>S. M. Sze, *Physics of Semiconductor Devices* (Wiley, New York, 1981).
- <sup>23</sup>N. W. Ashcroft and N. D. Mermin, *Solid State Physics* (Brooks-Cole, Belmont, MA, 1976).
- <sup>24</sup>J. H. Davies, *The Physics of Low-dimensional Semiconductors* (Cambridge University Press, Cambridge, 1998).
- <sup>25</sup>Y. Fukaya, A. Kawasuso, and A. Ichimiya, *e-J. Surf. Sci. Nanotechnol.* **3**, 228 (2005).
- <sup>26</sup>T. Heinzl, *Mesoscopic Electronics in Solid State Nanostructures* (Wiley, New York, 2003).
- <sup>27</sup>B. L. Altshuler, A. G. Aronov, and P. A. Lee, *Phys. Rev. Lett.* **44**, 1288 (1980).
- <sup>28</sup>H. Fukuyama, *J. Phys. Soc. Jpn.* **48**, 2169 (1980).
- <sup>29</sup>T. Ando, A. B. Fowler, and F. Stern, *Rev. Mod. Phys.* **54**, 437 (1982).
- <sup>30</sup>B. J. F. Lin, M. A. Paalanen, A. C. Gossard, and D. C. Tsui, *Phys. Rev. B* **29**, 927 (1984).
- <sup>31</sup>P. W. Anderson, E. Abrahams, and T. V. Ramakrishnan, *Phys. Rev. Lett.* **43**, 718 (1979).
- <sup>32</sup>M. Ono, Y. Nishigata, T. Nishio, T. Eguchi, and Y. Hasegawa, *Phys. Rev. Lett.* **96**, 016801 (2006).
- <sup>33</sup>R. S. Markiewicz and L. A. Harris, *Phys. Rev. Lett.* **46**, 1149 (1981).
- <sup>34</sup>C.-S. Jiang, X. Tong, S. Hasegawa, and S. Ino, *Surf. Sci.* **376**, 69 (1997).
- <sup>35</sup>S. Hasegawa, C.-S. Jiang, Y. Nakajima, and X. Tong, *Surf. Rev. Lett.* **5**, 803 (1998).
- <sup>36</sup>B. Abeles, P. Sheng, M. D. Coutts, and Y. Arie, *Adv. Phys.* **24**, 407 (1975).
- <sup>37</sup>V. Ambegaokar, B. I. Halperin, and J. S. Langer, *Phys. Rev. B* **4**, 2612 (1971).
- <sup>38</sup>N. F. Mott, *Philos. Mag.* **19**, 835 (1969).